

Mapping leaf chlorophyll and leaf area index using inverse and forward canopy reflectance modeling and SPOT reflectance data

Rasmus Houborg^{a,*}, Eva Boegh^b

^a USDA-ARS, Hydrology and Remote Sensing Laboratory, BARC-WEST, Beltsville, MD 20705, United States

^b Roskilde University, Universitetsvej 1, DK-4000 Roskilde, Denmark

Received 14 November 2006; received in revised form 17 April 2007; accepted 22 April 2007

Abstract

Reflectance data in the green, red and near-infrared wavelength region were acquired by the SPOT high resolution visible and geometric imaging instruments for an agricultural area in Denmark (56°N, 9°E) for the purpose of estimating leaf chlorophyll content (C_{ab}) and green leaf area index (LAI). SPOT reflectance observations were atmospherically corrected using aerosol data from MODIS and profiles of air temperature, humidity and ozone from the Atmospheric Infrared Sounder (AIRS), and used as input for the inversion of a canopy reflectance model. Computationally efficient inversion schemes were developed for the retrieval of soil and land cover-specific parameters which were used to build multiple species and site dependent formulations relating the two biophysical properties of interest to vegetation indices or single spectral band reflectances. Subsequently, the family of model generated relationships, each a function of soil background and canopy characteristics, was employed for a fast pixel-wise mapping of C_{ab} and LAI.

The biophysical parameter retrieval scheme is completely automated and image-based and solves for the soil background reflectance signal, leaf mesophyll structure, specific dry matter content, Markov clumping characteristics, C_{ab} and LAI without utilizing calibration measurements.

Despite the high vulnerability of near-infrared reflectances (ρ_{nir}) to variations in background properties, an efficient correction for background influences and a strong sensitivity of ρ_{nir} to LAI, caused LAI– ρ_{nir} relationships to be very useful and preferable over LAI–NDVI relationships for LAI prediction when LAI > 2. Reflectances in the green waveband (ρ_{green}) were chosen for producing maps of C_{ab} .

The application of LAI–NDVI, LAI– ρ_{nir} and C_{ab} – ρ_{green} relationships provided reliable quantitative estimates of C_{ab} and LAI for agricultural crops characterized by contrasting architectures and leaf biochemical constituents with overall root mean square deviations between estimates and in-situ measurements of 0.74 for LAI and 5.0 $\mu\text{g cm}^{-2}$ for C_{ab} .

The results of this study illustrate the non-uniqueness of spectral reflectance relationships and the potential of physically-based inverse and forward canopy reflectance modeling techniques for a reasonably fast and accurate retrieval of key biophysical parameters at regional scales.

© 2007 Elsevier Inc. All rights reserved.

Keywords: Leaf chlorophyll; Leaf area index; SPOT; AIRS; MODIS; Spectral reflectances; Canopy reflectance model; Inverse modeling; Atmospheric correction; Markov clumping; Leaf mesophyll structure; Dry matter content; Green reflectance; Near-infrared reflectance; NDVI; Image-based application; Maize; Barley; Wheat

1. Introduction

Accurate quantitative estimates of leaf biochemical and canopy biophysical variables are important for land surface models quantifying the exchange of energy and matter between the land surface and the lower atmosphere. Key variables

include the leaf area index (LAI), here defined as the single sided area of green, functioning leaves per unit ground, that exhibits a major control on transpiration and uptake of CO_2 by the canopy, and leaf chlorophyll content (C_{ab}) that can assist in determining photosynthetic capacity and productivity (e.g. Boegh et al., 2002; Nijs et al., 1995).

Remotely sensed data in the reflective optical domain function as a unique cost-effective source for a detailed knowledge of the spatial and temporal variations of these key canopy characteristics. The shape and form of canopy reflectance

* Corresponding author. Tel.: +1 301 504 8902; fax: +1 301 504 8931.

E-mail address: rasmus.houborg@ars.usda.gov (R. Houborg).

spectra depends on many factors such as vegetation structure, leaf biochemical composition, soil background, and the view and illumination geometry. For instance, LAI has a large impact on reflectance spectra especially in the near-infrared (NIR) while the visible part of the spectrum is strongly affected by leaf chlorophyll.

Remote sensing techniques to estimate vegetation characteristics from reflective optical measurements have either been based on the empirical–statistical approach that relates surface measurements of canopy variables to single spectral reflectances or vegetation indices (VI), or on the inversion of a physically based canopy reflectance (CR) model. Both approaches have their advantages and disadvantages. The potential of VIs for the determination of crop parameters have been demonstrated in numerous studies (e.g. Broge & Leblanc, 2001; Colombo et al., 2003; Gitelson et al., 2005; Tucker, 1980) and the simplicity and computational efficiency of the approach makes it highly desirable for large-scale remote sensing applications. However, a fundamental problem with the VI approach for estimating biophysical variables is its lack of generality. Since canopy reflectance depends on a complex interaction of several internal and external factors (Baret, 1991) that may vary significantly in time and space and from one crop type to another, no universal relationship between a single canopy variable and a spectral signature can be expected to exist. Consequently, spectral reflectance relationships will be site-, time- and crop-specific, making the use of a single relationship for an entire region unfeasible (Baret & Guyot, 1991; Colombo et al., 2003; Gobron et al., 1997).

The physically-based models have proven to be a promising alternative as they describe the transfer and interaction of radiation inside the canopy based on physical laws and thus provide an explicit connection between the biophysical variables and the canopy reflectance. Different strategies have been proposed for the inversion of these models including numerical optimization methods (e.g. Jacquemoud et al., 1995, 2000), look-up table approaches (e.g. Combal et al., 2002; Knyazikhin et al., 1998a,b; Weiss et al., 2000) and artificial neural network methods (e.g. Bacour et al., 2006; Fang & Liang, 2005; Walthall et al., 2004; Weiss & Baret, 1999). Look-up table and neural network approaches require a training database consisting of canopy reflectance spectra together with the corresponding biophysical variables, and their performances rely on the training database and the training process itself. Ideally, these approaches should be learned on experimental data which is not readily available for most places on the globe. The iterative optimization approach facilitates a direct retrieval of biophysical parameters from observed reflectances without the prior use of calibration or training data of any kind. However, this method suffers from its expensive computational requirement (Jacquemoud et al., 2000) making the retrieval of biophysical variables unfeasible for large geographic areas. A limitation shared by all of the physically-based models is the ill-posed nature of model inversion (Atzberger, 2004; Combal et al., 2002); the fact that different combinations of canopy parameters may correspond to almost

similar spectra. This makes the choice of the initial parameter values important, and some regularization of the inverse problem may be required implying the use of a priori knowledge or information on the spatial or temporal variability of key canopy parameters to constrain the inversion process (Atzberger, 2004; Combal et al., 2002; Houborg et al., 2007).

The crop-specific sensitivity of spectral reflectance relationships to canopy geometry (e.g. leaf angle distribution and clumping) and leaf properties (e.g. dry matter and mesophyll structure) and the site-specific sensitivity to atmospheric and background influences must be properly accounted for in order to apply spectral reflectance relationships for the mapping of LAI and C_{ab} . In this study inverse and forward CR modeling techniques were combined for a pixel-wise estimation of LAI and C_{ab} from a family of spectral reflectance relationships. The relationships were derived separately for pre-classified land cover classes due to the dependence on land cover-specific parameters and were also made dependent on the soil background reflectance signal. To make LAI and C_{ab} estimates independent of in-situ and calibration data, the crop and site-specific parameters needed to build the appropriate spectral reflectance relationships were retrieved from the inversion of a CR model employing the iterative optimization approach. Since the inversion of the CR model is computationally demanding the inversions were performed using reflectance observations averaged over several pixels. Additionally, pixel-wise inversions for the retrieval of LAI and C_{ab} were avoided making the scheme applicable for regional-scale use.

While the use of VI rather than single spectral reflectance relationships for estimating biophysical parameters tends to reduce the sensitivity to internal and external factors such as background and atmospheric influences, the translation of spectral reflectance data into a VI may also reduce the sensitivity to the parameter of interest. For instance, the widely used Normalized Difference Vegetation Index (NDVI) that combines reflectances in the near-infrared (NIR) and red waveband approaches a saturation level at intermediate values of LAI while NIR band reflectances remain sensitive to LAI in densely vegetated areas (e.g. Huete et al., 2002; Knyazikhin et al., 1998a). Several studies have demonstrated a maximum sensitivity of reflectances in the green (540–560 nm) and red edge (700–730 nm) spectrum to changing leaf chlorophyll concentrations (e.g. Gitelson et al., 1996; Gitelson et al., 2005; Houborg et al., 2007; Yoder & Pettigrew-Crosby, 1995). However, VIs that combine leaf chlorophyll sensitive reflectances and ρ_{nir} , which is highly responsive to changing leaf biomass, are typically not correlated with leaf chlorophyll content due to a high variability of ρ_{nir} relative to chlorophyll sensitive reflectance data (Boegh et al., 2002). In this study, the use of NIR band reflectances as predictors of LAI for intermediate to high vegetation densities was investigated while NDVI relationships were adopted for low vegetation densities. The mapping of leaf chlorophyll rather than total canopy chlorophyll was facilitated using relationships based on reflectances from the green waveband.

In this particular study, the turbid medium Markov chain CR model developed by Kuusk (1995, 2001) coupled to the

PROSPECT leaf optics model (Baret & Fourty, 1997; Jacquemoud & Baret, 1990) was adopted for the biophysical parameter retrievals using input of SPOT reflectance observations. Accurate reflectance input data are a prerequisite for a successful retrieval of biophysical parameters from physically based CR models. Consequently, the feasibility of aerosol data from MODIS and atmospheric profiles of air temperature, humidity and ozone from the Atmospheric Infrared Sounder (AIRS) for the atmospheric correction of SPOT radiances was explored. The estimates of LAI and C_{ab} were validated using field measurements from a number of agricultural sites.

2. Field experiment

A field experiment was conducted from early May through late September, 2005 in affinity to The Danish Institute of Agricultural Sciences, which is located in an agricultural area near Viborg in Denmark (9.423 E, 56.486 N). Denmark is located in the zone of prevailing westerlies causing a temperate and fairly humid environment. The precipitation total for the study period was 313 mm and the warmest months were July and August with daily mean temperatures of 17.5 °C and 16.1 °C, respectively (Denmark's Meteorological Institute, 2006). Field data of leaf chlorophyll and leaf area index were collected on fields of barley, wheat and maize throughout the experiment and spectral reflectance observations for a 60×60 km image swath were acquired in June, September and October by SPOT satellite sensors.

2.1. Biophysical measurements

A portable SPAD-502 chlorophyll meter (Minolta, Spain) was used for non-destructive measurements of leaf chlorophyll. However, in order to use the unit-less SPAD values for validating satellite-based leaf chlorophyll estimates a relationship with leaf chlorophyll must be initially established. For this purpose a total of 18 barley, wheat and maize leaf samples were thoroughly measured with the SPAD-502 and subsequently cut into 1–2 cm pieces and kept frozen until measurement time. The chlorophyll (a+b) content was extracted using the common *N,N*-dimethylformamide solvent method (e.g. Moran, 1992). Extinction coefficients published by Porra et al. (1989) for chlorophyll pigments diluted in *N,N*-dimethylformamide were used for calculating the concentrations. All results are means of duplicate (×2) determinations on duplicate field samples.

While the relationship between leaf chlorophyll content and the output of a SPAD-502 meter will vary from meter to meter, the determination of leaf chlorophyll from the same SPAD-502 meter appears to be rather independent of species (Markwell et al., 1995). This was also confirmed from the inspection of our data for barley, wheat and maize leaves and as theoretically justified by Markwell et al. (1995) an exponential equation was found to best describe the relationship between the calculated chlorophyll concentrations and the SPAD-502 measurements. The relationship used to convert

SPAD-502 field measurements into leaf chlorophyll content ($\mu\text{g cm}^{-2}$) reads

$$C_{ab} = 6.34299 \cdot \exp(\text{SPAD} \cdot 0.04379) - 6.10629 \quad (\text{RMSD} = 5.4 \mu\text{gcm}^{-2}). \quad (1)$$

Leaf chlorophyll and LAI validation data were collected in field plots sown with barley (6), wheat (5) and maize (18) respectively. Measurements were collected throughout the growing season at 8 field plots each having a size of 10 m×10 m, and supplementary data were collected in 21 smaller plots (3 m×3 m) during the mid-growing period where vegetation density is highest. Leaf chlorophyll measurements were conducted with the SPAD meter at 10 cm increments from the bottom to the top of the green layer, and a bulk value was derived by integration of the profile data. In the large field plots, 50–150 SPAD measurements provide the data basis to estimate leaf chlorophyll, and in the smaller plots, 10–15 SPAD measurements were used. Each leaf measurement was duplicated to allow detection and removal of bad data. Measurements were made in conjunction with non-destructive LAI estimates (LAI-2000, LI-COR, USA) which were based on recordings every 1.5 m along two full-length transects located perpendicular to each other within each field plot. The field plots are randomly distributed within an area of 10 km×10 km.

3. Satellite data acquisition and processing

Reflectance data in the green, red and near-infrared wavelength regions were acquired by SPOT high resolution visible and geometric imaging instruments (Section 3.3). SPOT spectral radiances were converted to reflectances using the atmospheric transfer model MODTRAN 4.0 with input of atmospheric aerosol concentration from the MODerate resolution Imaging Spectroradiometer (MODIS) (Section 3.1) and atmospheric profiles of air temperature, humidity and ozone from the Atmospheric InfraRed Sounder (AIRS) (Section 3.2) acquired from the EOS Data Gateway (<http://deleenn.gsfc.nasa.gov/~imswww/pub/imswelcome>).

MODIS, AIRS and SPOT data were geometrically rectified and co-registered in UTM coordinates (UTM zone 32, Datum WGS-84). A digital road network map from the Danish Areal Information System (AIS, 2000) was used to improve the geolocation accuracy of the high-resolution SPOT scenes.

3.1. MODIS aerosol data

For atmospheric correction purposes and for calculating the diffuse fraction of incoming solar radiation (Section 4.2), aerosol optical thicknesses (τ) at 0.47 and 0.66 μm were acquired from the Aqua MODIS aerosol product (MYD04). The aerosol properties are reported at 10 km resolution and are derived by inversion of MODIS observed reflectances at 500 m resolution using pre-computed radiative transfer look-up tables based on dynamical aerosol models (Kaufman et al., 1997). Product MYD04 is in a stage 2 validation (stage 3 represents the highest degree of product confidence) and the MODIS

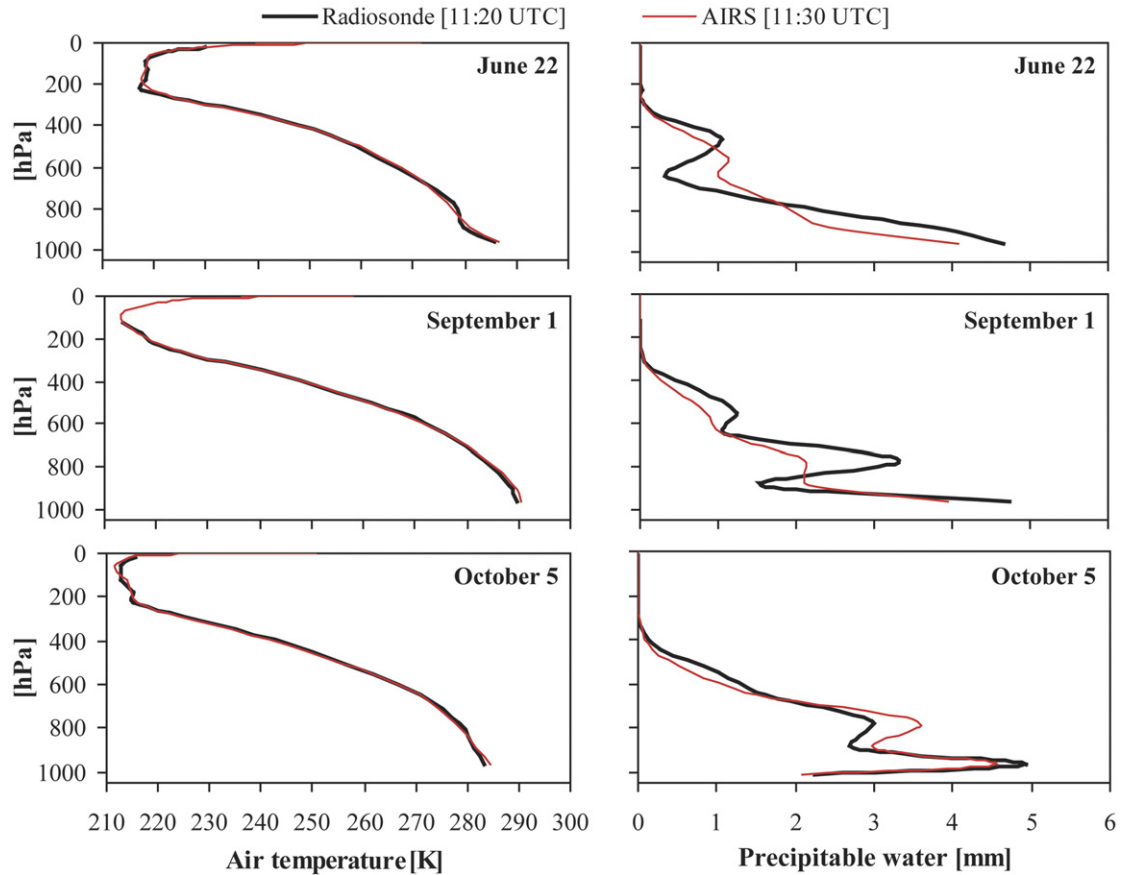


Fig. 1. Profile comparisons of AIRS and radiosonde atmospheric temperature and humidity at the days of the three SPOT acquisitions (Section 3.3). The radiosondes were released from Jægersborg, Denmark (55.77 °N, 12.52 °E) at 11:20 UTC, which is very close to the AIRS overpass time.

Algorithm Theoretical Basis Document (Kaufman & Tanré, 1998) reports a predicted uncertainty of $\pm 0.05 \pm 0.2\tau$ which appears to be a reasonable uncertainty estimate for green vegetated surfaces (Houborg et al., accepted for publication; Vermote et al., 2002). While the aerosol observations were acquired approximately an hour later than the SPOT reflectance observations (Section 3.3), comparisons of aerosol optical thicknesses at the Aqua (~11:30 UTC) and Terra overpass times (~9:45 UTC) at the days of the SPOT acquisitions indicated a daily temporal variability in τ of less than 0.013 (not shown). The largest source of error is more likely the algorithm estimation uncertainty (i.e. $\pm 0.05 \pm 0.2\tau$). The impact of the τ uncertainty on surface reflectance retrieval was examined by Vermote and Vermeulen (1999) who reported typical absolute errors of green reflectance of 0.003 and 0.007, and NIR reflectance of 0.008 and 0.018 for $\tau_{0.55}$ values of 0.1 and 0.5, respectively.

3.2. AIRS atmospheric profiles

Atmospheric profiles of retrieved temperature, humidity and ozone were extracted from the AIRS level 2 Standard Retrieval Product and used as inputs to the MODTRAN atmospheric radiative transfer model. AIRS data were preferred over localized radiosonde observations that are only available at widely separated sites and therefore may not be representative of the

atmospheric conditions of the area to be mapped. The Standard Product contains quality assessment flags in addition to the retrieved quantities that are reported at 28 pressure levels ranging from 1100 mb to 0.1 mb.

Temperature and humidity retrievals were previously only validated for non-polar regions ($|\text{lat}| \leq 50^\circ$) over land and ocean. Atmospheric temperature and water vapor profiles appear to be well characterized over the ocean meeting RMSD difference specifications of ~1 K and 15%, respectively while larger uncertainties exist over land in the bottom 2 km of the profile (Fetzer et al., 2005). In order to evaluate the performance of AIRS temperature and water vapor profiles for Denmark, they were compared with radiosonde observations provided by the

Table 1

Agreement between AIRS and radiosonde observations of air temperature and total precipitable water (TPW) expressed in terms of root mean square deviations (RMSD) and bias

Air temperature	RMSD [K]	Bias [K]
1013–750 mb	1.07	0.4
750–250 mb	0.78	-0.39
<250 mb	1.06	-0.28
	RMSD [mm]	Bias [mm]
TPW	1.6	-1.4

Danish Meteorological Institute for the same geographical location (55.77° N, 12.52° E) at the days of the SPOT acquisitions. Temperature retrievals compare very well with the radiosonde observations throughout the atmospheric column (Fig. 1) with RMS deviations of around 1 K (Table 1). AIRS water vapor retrievals are characterized by larger uncertainties (Fig. 1). Still the general trend in the water vapor profile is well captured and the RMS deviation is only 1.6 mm for retrieved total water vapor (Table 1). Larger uncertainties in profile estimates may be anticipated in regions with strong surface heating (Fetzer et al., 2005). Atmospheric profile measurements of ozone were not available for verification of the AIRS estimates. However, AIRS total ozone contents at the days of the SPOT acquisitions compared favorably with monthly mean observations reported by Denmark's Meteorological Institute (Denmark's Meteorological Institute, 2006).

3.3. SPOT reflectance data

Radiances in the green (500–590 nm), red (610–680 nm) and near-infrared (780–890 nm) wavelength regions were obtained in 20 m resolution on June 22 and 10 m resolution on September 1 and October 5, 2005 by the SPOT 3 high resolution visible (HRV) and SPOT 5 geometric imaging (HRG) instruments, respectively for 60 km × 60 km image swaths. The mid-infrared band (1580–1750 nm) available on SPOT 5 was not included in the present analysis as this band is not present on SPOT 3. However, the atmospheric correction procedure has been setup to correct for atmospheric water vapor absorption in the mid-infrared wavelength region to accommodate future applications of the model with the mid-infrared band present.

The atmospheric conditions at the Aqua overpass times (11:30, 11:35 and 11:25 UTC) were assumed to be representative of the atmospheric conditions at the time of the SPOT overpasses (10:32, 10:14 and 10:59 UTC) since they were only approximately an hour apart. Thus MODTRAN was run with inputs of the appropriate spectral filter response functions, Aqua MODIS aerosol data, and Aqua AIRS profile retrievals of air temperature, humidity and ozone. The atmospheric model was run in multiple-scattering mode to establish a linear function between the radiance recorded by the sensor and the spectral (assumed Lambertian) surface reflectance.

Since all of the agricultural crops in the region were either harvested or in a stage of senescence at the time of the October overpass, only the June and September acquisitions were used as input to the biophysical parameter retrieval scheme (Section 4). However all three scenes were used for the classification of land covers (Section 3.4).

3.4. Land cover classification

A land cover classification was produced to identify functionally similar vegetation classes required for the generation of a suite of land cover-specific relationships between the two biophysical properties of interest and spectral band reflectances (Section 4). An unsupervised isodata classification approach was adopted. The combined use of NDVI and near-

Table 2

Agricultural land cover classes identified by the unsupervised isodata classification

Land cover class	% of total land area	Classification accuracy [%]
1 Wheat	6.3	95.5
2 Barley	11.9	89.6
3	7.4	
4	5.9	
5 Maize	4.0	97.9
6	5.2	
7	3.2	
8	3.0	
9 Grass	6.7	99.5
10 Maize (<i>late sown</i>)	2.3	97.9
11	1.8	
12 Barley (<i>with catch crop</i>)	4.2	89.6
13	3.7	
	65.6	97.0

The vegetation types have been assigned on the basis of ground-truth reference data. The assignment of specific crop types to the spectrally separate classes allows crop-specific leaf inclination angles to be set a priori if known (Section 4.2); otherwise a spherical distribution is assumed. The class percentages of the total land area within the SPOT scene are provided along with the classification accuracy.

infrared reflectance images from all three SPOT scenes was found to be optimal for the separation of classes. A vector map from the Danish Areal Information System (AIS, 2000) was used for the identification of urban areas and road networks. The isodata classification is based on a number of input threshold parameters (Tou & Gonzalez, 1974), such as the minimum and maximum number of classes to define, and for the studied region a total of 13 spectrally separate agricultural classes were generated. While some classes may belong to the same crop type, within crop spectral signature differences could be an indication of variations in the biophysical properties. The consideration of class-specific biophysical properties is a key element in the inversion scheme (Section 4.4). An overall classification accuracy of 97 % was calculated using confusion matrices and ground-truth reference data collected from 30 fields representing wheat, barley, maize and grass (Table 2). The assignment of specific crop types to the spectrally separate classes is not a prerequisite for implementing the model but allows crop-specific leaf inclination angles to be set a priori if known (Section 4.2); otherwise a spherical distribution is assumed.

4. Biophysical parameter retrieval scheme

A schematic diagram of the satellite-based biophysical parameter retrieval scheme is given in Fig. 2 Spatial maps of LAI and C_{ab} were generated using spectral reflectance relationships established by running a canopy radiative transfer model (Section 4.1) in forward mode. The relationships were derived separately for pre-classified land cover classes to account for the land cover-specific sensitivity to canopy geometry (leaf angle distribution and clumping) and leaf optical properties (dry matter content and mesophyll structure), and were also made dependent on site-specific factors (soil

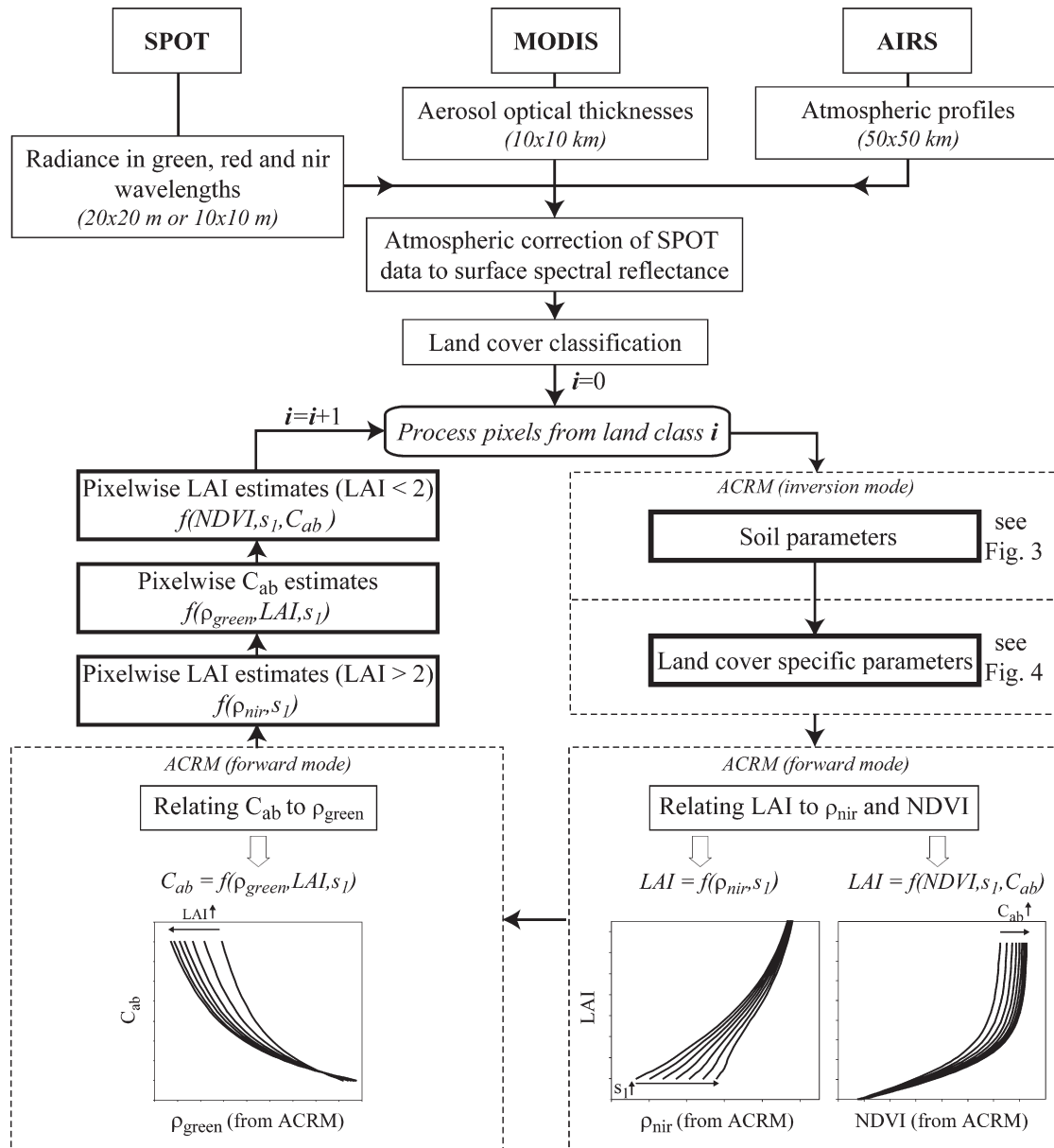


Fig. 2. A schematic diagram of the satellite-based biophysical parameter retrieval scheme. Inverse and forward canopy reflectance modeling techniques were combined for the retrieval of LAI and leaf chlorophyll content (C_{ab}) using SPOT green (ρ_{green}), red (ρ_{red}) and near-infrared (ρ_{nir}) reflectance observations.

reflectance). Land cover and site-specific parameters were derived using inverse canopy reflectance modeling (Sections 4.3 and 4.4). The retrieval scheme requires two clear-sky SPOT scenes to represent conditions of dense green vegetation and bare soil respectively for each of the agricultural classes of interest.

4.1. Canopy radiative transfer model

The turbid medium Markov chain canopy reflectance model, ACRM (Kuusk 1995, 2001) was chosen for the retrieval of biophysical parameters using the SPOT surface reflectance input dataset (Section 3.3). The ACRM incorporates Markov properties of stand geometry making it applicable to plant canopies largely made up of vertical elements such as corn

(Kuusk, 1995). In the ACRM the canopy is supposed to consist of a homogeneous layer of vegetation and a thin layer of vegetation on the ground surface.

The model operates in the spectral domain 400–2500 nm and computes directional canopy reflectance at a spectral resolution of 1 nm. The model inputs are listed in Table 3. The angular distribution of leaves is described by the modal leaf inclination (θ_m) and the eccentricity (e_L) in accordance with an elliptical leaf angle distribution (LAD). However as a simplification, the mean leaf inclination angle (θ_1) was used to parameterize e_L and θ_m in accordance with an ellipsoidal LAD (Campbell, 1990), which implies considering only planophile and erectophile modal leaf orientations ($\theta_m=0$ and $\theta_m=90$, respectively). The model accounts for non-lambertian soil reflectance and the spectral variability of soil reflectance is

Table 3
Input parameters required to run the canopy reflectance model

Parameters	Units	Symbol	Range or fixed value
<i>External parameters</i>			
Angstrom turbidity coefficient		β	0.11, 0.24
Sun zenith angle	(°)	SZA	34.1, 49.5
Relative azimuth angle	(°)	RAZ	96.6, 99.9
View zenith angle	(°)	VZA	10.7, 30.3
<i>Canopy structure parameters</i>			
Leaf area index		LAI	0–8
Markov clumping parameter		S_z	0.4–1.0
Hot spot parameter		S_L	0.5/LAI
Mean leaf inclination angle	(°)	θ_1	57 ^a
LAI of the ground level		LAI _g	0.1
<i>Soil parameters</i>			
Weight of the first price function		s_1	0–0.7
Weight of the second price function		s_2	–0.1–0.1
<i>Leaf biochemical constituents</i>			
Chlorophyll <i>a+b</i> content	$\mu\text{g}/\text{cm}^2$	C_{ab}	10–100
Leaf equivalent water thickness	cm	C_w	0.02
Dry matter content	g/m^{-2}	C_m	20–100
Brown pigment concentration		C_{bp}	0.0005
Leaf mesophyll structure		N	1–3

The dry matter and leaf chlorophyll content are given per unit leaf area. Where two values are given, the first applies to the June overpass (22.06.2005) while the latter applies to the September overpass (01.09.2005). For the inverse estimation of soil parameters (Section 4.3) the vegetation parameters were set to the midpoints of the effective ranges for all land cover classes.

^a Unless known a priori.

approximated as a function of four vectors according to Price (1990). However, only the two first vectors were used in the inversion as they explain as much as 94.2% of the spectral variability in the soil reflectance (Price, 1990). Additionally, the specular reflection of direct sun radiation on leaves and the hot spot effect are accounted for.

In the ACRM, the spectra of leaf reflectance and transmittance are computed using the most recent version of the leaf optics model PROSPECT (Baret & Fourty, 1997; Jacquemoud & Baret, 1990). In PROSPECT the leaf scattering is described by the leaf mesophyll structure (N) and a tabulated wavelength dependent refractive index of the leaf surface wax while leaf absorption is calculated as a function of four biochemical constituents (Table 3).

The inversion of ACRM for the retrieval of two or more model parameters consists in minimizing the merit function (Kuusk, 2003) defined as

$$F(\mathbf{x}) = \sum \left(\frac{\rho_j^* - \rho_j}{\varepsilon_j} \right)^2 + \sum \left[(x_i - x_{i,b})^4 w_i^2 \right] \quad (2)$$

where \mathbf{x} is the vector of model input parameters (x_1, x_2, \dots, x_n), ρ_j^* is the observed reflectance, ε_j is the error of ρ_j^* , ρ_j is the simulation model reflectance estimate, n is the number of reflectance samples, w_i is a weight, and $x_{i,b}$ is the value of x_i on the boundary of the given region (see Table 3 for range values). Thus the merit function accounts for uncertainties in the reflectance data and avoids the non-physical values of input

parameters. The Powell minimization technique is used to solve the multi-dimensional function (Kuusk, 2003).

4.2. Model inputs and parameterization

Input parameters required for the canopy radiative transfer model are listed in Table 3. The external parameters constitute atmospheric and view geometry information (Table 3) and represents conditions at the acquisition of the spectral surface reflectances at the two SPOT overpass days. The Ångström turbidity coefficient (β), which is needed to compute the diffuse fraction of incoming radiation, was estimated from Ångström's turbidity formula (Iqbal, 1983) using inputs of aerosol optical thicknesses at 0.47 ($\tau_{0.47}$) and 0.66 μm ($\tau_{0.66}$) which were acquired from the MODIS aerosol product (Section 3.1).

The hot spot parameter (S_L) was parameterized as a function of LAI according to Verhoef and Bach (2003). For wheat, barley and maize canopies, leaf inclination angles measured in the field using a LI-2000 were assumed to apply ($\theta_1=62^\circ$, 66° and 50° respectively). For the remaining land cover classes a spherical leaf angle distribution was assumed ($\theta_1=57^\circ$), which is the model default if a crop type is not assigned to a land cover class. The setting of the leaf equivalent water thickness (Table 3) is not important since leaf water has no effect on the reflectance in the visible and near-infrared wavebands (e.g. Houborg et al., 2007).

In total, 7 free model parameters remain; leaf area index (LAI), leaf chlorophyll content (C_{ab}), dry matter content (C_m), Markov clumping parameter (S_z), leaf mesophyll structure (N), and the two soil parameters (s_1 and s_2) (Table 3). The retrieval scheme was further regularized by assuming C_m , S_z and N to be invariant within each land cover class. Inverse model estimation of class-specific (C_m , S_z and N) biophysical properties and site-specific soil parameters (s_1 and s_2) are outlined in the next two sections. The methodology employed for the pixel-wise mapping of LAI and C_{ab} is elucidated in Section 4.5.

4.3. Inverse estimation of soil parameters

The s_1 and s_2 retrieval scheme (Fig. 3) incorporates a land cover map (Section 3.4) in addition to a soil map from the Danish Institute of Agricultural Sciences (1996) that distinguishes between 6 different soil types. The steps detailed in Fig. 3 were done separately for each of the spectrally separate land cover classes, and the existence of 'bare soil' pixels (i.e. LAI<0.5) is a pre-requisite for reliable retrievals of s_1 and s_2 . This implies that for each land cover, a satellite scene containing bare soil or low vegetation density is selected for the inverse retrieval of permanent site-specific soil parameters.

The scheme assumes that (1) default vegetation parameter values (Table 3) can be used irrespective of land cover class as the setting of these parameters will have a minor influence on the reflectance signal for "bare soil" pixels and (2) the soil color of individual pixels is similar at the time of the SPOT acquisitions, which is a valid assumption when the humus content remains unchanged and the topsoil is equally dry in all scenes. This latter assumption facilitates the use of the same soil parameter maps (Fig. 3) for both SPOT scenes.

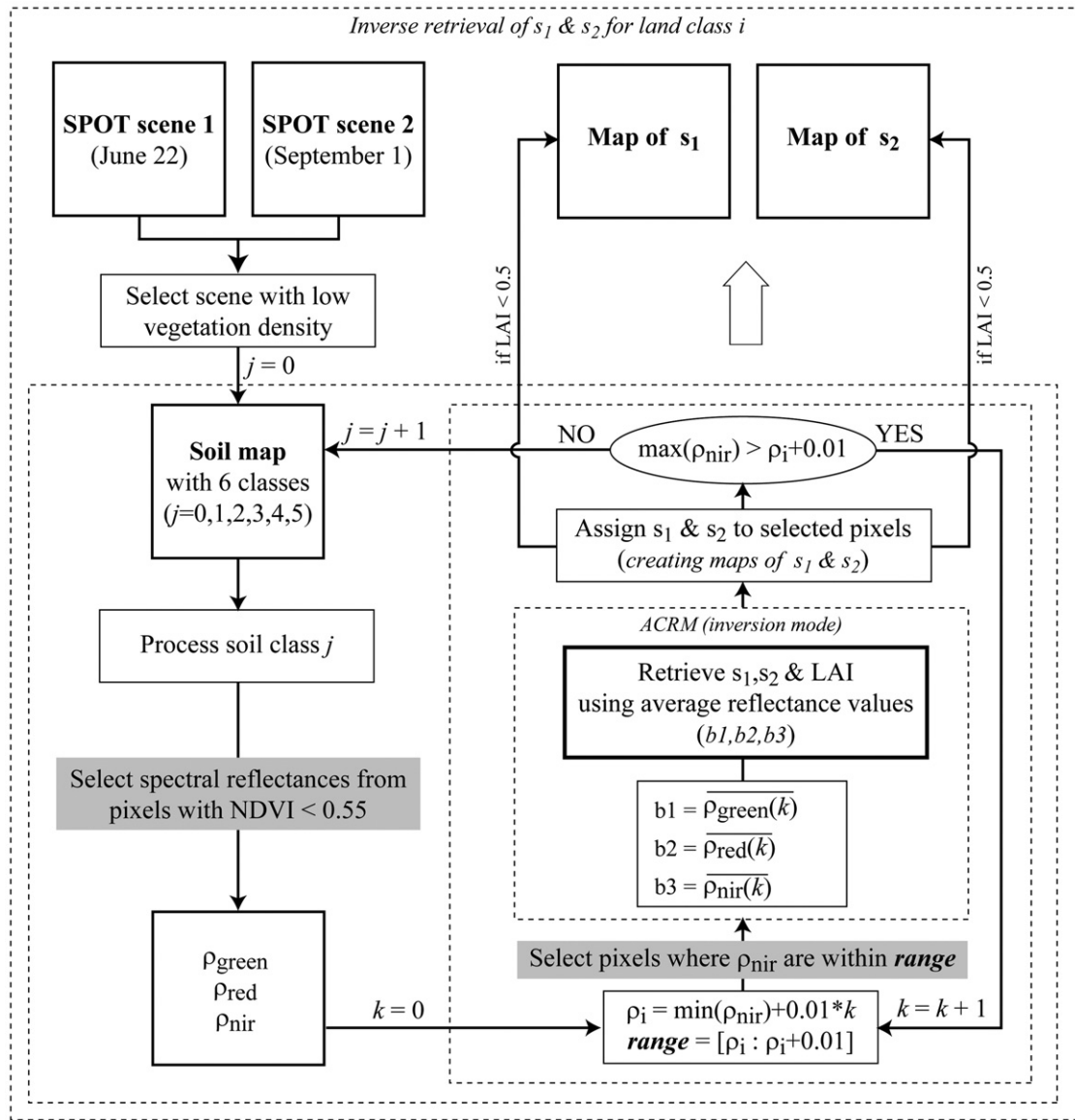


Fig. 3. A schematic diagram of the scheme developed for a reasonably fast inverse retrieval of the two soil coefficients (s_1 and s_2) that describe the spectral variability of the soil reflectance. The illustrated actions were performed independently for each land cover class, which implies that for each land cover, a satellite scene containing bare soil or low vegetation density is selected for the inverse retrieval of permanent soil parameters.

Since a pixel-wise retrieval of s_1 and s_2 using inverse ACRM modeling would be very time consuming for regional-scale applications, inverse ACRM modeling was applied on a limited number of averaged spectral reflectance values.

In the selected low vegetation density scene (for the given land cover class), a NDVI threshold of 0.55 was applied as a first step to exclude pixels, with a too high contaminating vegetation signal, from the analysis (Fig. 3). The observed range in the selected ρ_{nir} values was then sub-divided in intervals of width 0.01, which provided a good compromise between computational speed and spatial representation. Subsequently, all NIR and corresponding green and red reflectance observations within each sub-range were averaged, and the averaged spectral reflectance values used as input to the ACRM for the inverse retrieval of s_1 , s_2 and LAI using default parameter values for all

remaining parameters (Table 3). LAI was included as a free variable to detect any contaminating vegetation signal, and the s_1 and s_2 retrievals were only assigned to the selected pixels if modeled $LAI < 0.5$ (Fig. 3).

In some cases, the retrieval of soil coefficients was not possible due to the presence of vegetation ($LAI > 0.5$) in both scenes. The pixel-wise retrievals of s_1 and s_2 were averaged for each soil type and the soil-specific estimates were extrapolated to the unfilled pixels using the soil map.

Since the second soil parameter, s_2 , only accounts for approximately 20% of the spectral variability in the soil reflectance (Price, 1990), land cover averaged rather than the pixel specific s_2 values were used for the pixel-wise mapping of LAI and C_{ab} (Section 4.5) in order to improve the computational efficiency of the approach.

4.4. Inverse estimation of class-specific parameters

An inversion scheme was designed to provide reasonably fast estimates of class-specific parameters (C_m , S_z and N) using multiple spatially averaged green, red and NIR reflectance observations during conditions of medium to high density vegetation coverage ($NDVI > 0.65$) (Fig. 4). The scheme exploits the information content provided by a spatial reflectance dataset. The steps detailed in Fig. 4 were done separately for each of the spectrally separate land cover classes, which implies that for each land cover, a satellite scene containing dense vegetation cover is selected and used for the inverse estimation of permanent vegetation parameters.

The assumed invariance of C_m , S_z and N within well-defined land cover classes makes the simultaneous use of multiple spatially distributed reflectance observations for the inverse retrieval of class-specific parameters feasible. The number of spatially averaged reflectance sets is chosen to represent the variations within the range of observed spectral reflectance for each land cover class. In this study, 8 sets of averaged

reflectances (8×3 spectral reflectances in total) were used. Only pixels completely surrounded by pixels of the same land cover class were included to avoid the use of mixed pixels. Additionally, extreme values were avoided due to possible contamination.

In each land cover-specific inversion, C_m , S_z , N , LAI and C_{ab} are unknown parameters. However since only a few parameters should be estimated simultaneously using numerical optimization techniques (Kuusk, 2003) and the ill-posed nature of model inversion (Atzberger, 2004; Combal et al., 2002) makes the setting of the initial parameter values important, only LAI and C_{ab} were subject to estimation in inversions initialized with all possible combinations of the C_m , S_z and N parameter values (Fig. 4). The set of C_m , S_z and N resulting in the best fit, in terms of the RMS deviation, between observed and calculated reflectances was assumed to apply to the respective land cover class.

Since LAI and C_{ab} may vary significantly within each land cover class, relationships were established to describe the relative spatial variability in LAI and C_{ab} between the 8 sets of

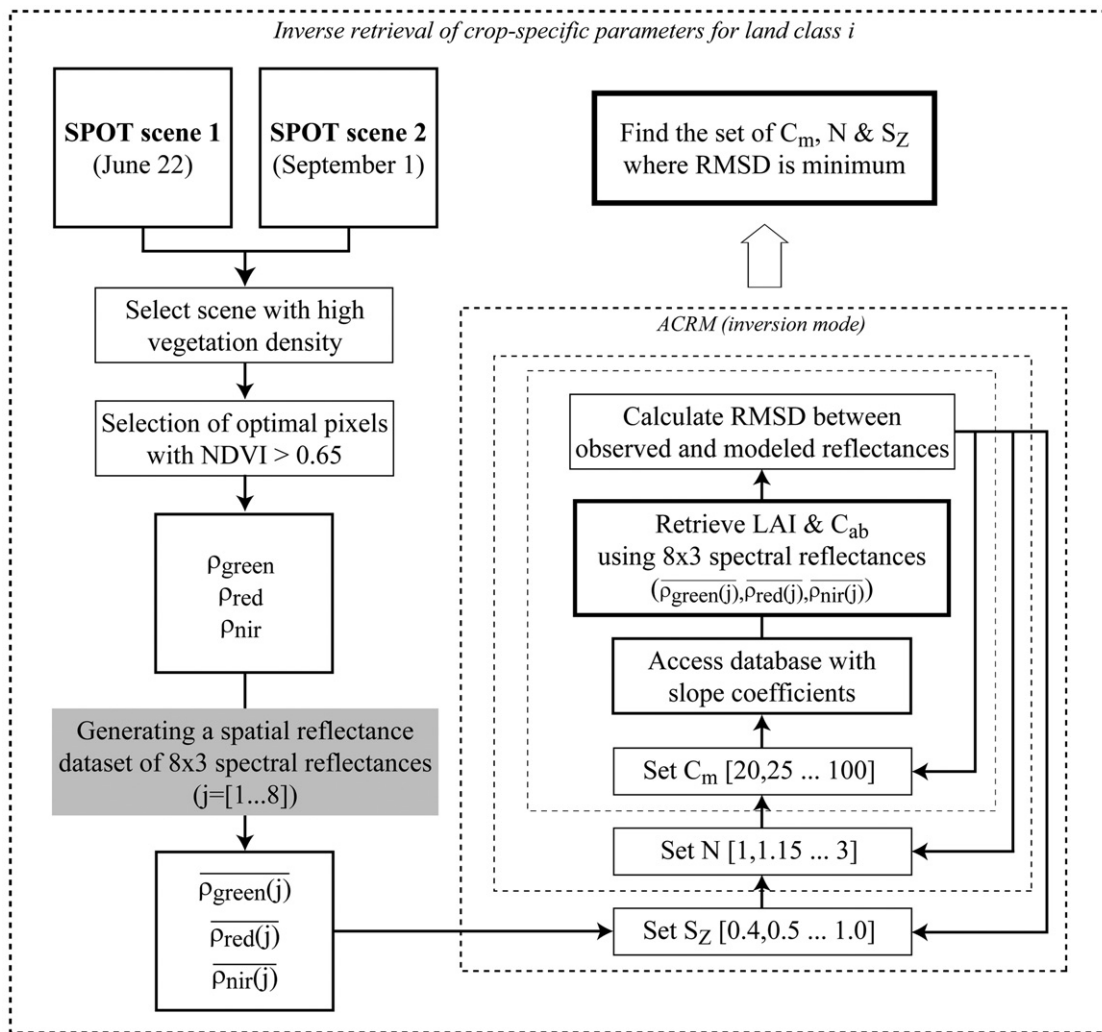


Fig. 4. A schematic diagram of the scheme developed for reasonably fast inverse retrievals of the dry matter content (C_m), leaf mesophyll structure (N) and Markov clumping parameter (S_z) assumed spatially invariant within each land cover class. The illustrated actions were performed independently for each land cover class, which implies that for each land cover, a satellite scene containing dense vegetation cover is selected and used for the inverse estimation of permanent vegetation parameters.

reflectances. For this purpose the ACRM was run in forward mode using all possible combinations of LAI, C_{ab} , C_m , S_z , θ_1 and N to construct a database of cubic polynomial coefficients describing the relationship between LAI and ρ_{nir} and between C_{ab} and ρ_{green} . In the inversion, the LAI variability between the individual sets of reflectances (i) was then approximated according to

$$\text{LAI}(i) = \overline{\text{LAI}} + a_1[\rho_{nir}(i) - \overline{\rho_{nir}}] + a_2[\rho_{nir}(i)^2 - \overline{\rho_{nir}^2}] + a_3[\rho_{nir}(i)^3 - \overline{\rho_{nir}^3}] \quad (3)$$

where $\overline{\text{LAI}}$ is the inverse LAI estimate representative of the entire spatial reflectance dataset, a_1 , a_2 and a_3 are the coefficients of the appropriate cubic polynomial relating LAI to ρ_{nir} (from the database of coefficients), and $\overline{\rho_{nir}}$ is the average NIR reflectance.

The variability in C_{ab} between the individual reflectance datasets was approximated in a similar way using green reflectances according to

$$C_{ab}(i) = \overline{C_{ab}} + b_1[\rho_{green}(i) - \overline{\rho_{green}}] + b_2[\rho_{green}(i)^2 - \overline{\rho_{green}^2}] + b_3[\rho_{green}(i)^3 - \overline{\rho_{green}^3}] \quad (4)$$

where b_1 , b_2 and b_3 are the coefficients of the appropriate cubic polynomial relating C_{ab} to ρ_{green} .

4.5. Pixel-wise estimation of LAI and C_{ab}

With the class-specific fixation of C_m , S_z and N completed, the ACRM was run in forward mode to generate a family of spectral reflectance relationships, each a function of the background reflectance signal and canopy characteristics, required for a fast pixel-wise mapping of LAI and C_{ab} (Fig. 2).

For each land cover class, the ACRM was run with variable input of LAI (0, 0.5 ... 8), s_1 (0.10, 0.13 ... 0.7) and C_{ab} (10, 15 ... 100), and ρ_{green} , ρ_{nir} and NDVI were output for each combination of this input data. The LAI data were then related separately to ρ_{nir} and NDVI using polynomial and exponential fitting, respectively and regression coefficients were derived for each value of s_1 and C_{ab} (for NDVI) to reflect differences in the relationships caused by variations in the soil background reflectance and leaf chlorophyll (for NDVI). Since ρ_{nir} is highly sensitive to the background reflectance signal for low vegetation densities, LAI–NDVI relationships were employed for pixels where $\text{LAI} < 2$, while LAI– ρ_{nir} relationships were adopted for the remaining pixels as ρ_{nir} contrary to NDVI remains sensitive to LAI in densely vegetated areas and in addition is unaffected by leaf chlorophyll variations (Houborg et al., 2007).

Similarly, C_{ab} was related to ρ_{green} using polynomial fitting and regression coefficients were derived for each value of s_1 and LAI. The fits were near-perfect with errors on the order of

0.1 for the LAI– ρ_{nir} and LAI–NDVI relationships and $0.5 \mu\text{g cm}^{-2}$ for the C_{ab} – ρ_{green} relationships.

A look-up table approach was adopted for mapping LAI and C_{ab} using the derived spectral reflectance relationships. The pixel-wise estimates of s_1 (Section 4.3) were first grouped into s_1 sub-intervals of width 0.015. The LAI– ρ_{nir} relationship appropriate to the specific s_1 -interval was then applied to all the pixels within the given s_1 class. Subsequently, the LAI estimates were grouped into a number of classes each representing a LAI sub-interval with a range of 0.5. This allows LAI to be estimated using a separate LAI–NDVI relationship for each combination of the s_1 and LAI classes. Finally, the C_{ab} estimates were grouped into a number of classes each representing a C_{ab} sub-interval with a range of $5 \mu\text{g cm}^{-2}$. This allows LAI to be estimated using a separate LAI–NDVI relationships for each combination of the s_1 and C_{ab} classes (Fig. 2).

5. Results

5.1. The effect of land cover

LAI– ρ_{nir} , LAI–NDVI and C_{ab} – ρ_{green} relationships were established independently for 13 spectrally classified agricultural land cover classes (Table 2) to reflect any between class variability in canopy architecture and leaf biochemical constituents.

The inverse estimates of the dry matter content (C_m), leaf mesophyll structure (N) and Markov clumping parameter (S_z) for the agricultural land cover classes are listed in Table 4. The dry matter content results for the 13 land cover classes lie in the interval 20–80 g m^{-2} (Table 4) with a mean value of 38 g m^{-2} which is slightly lower than the average (42 g m^{-2} , range: 22–101 g m^{-2}) obtained from 12 leaf samples representative of agricultural crops (predominantly maize) collected during the Leaf Optical Properties Experiment (LOPEX'93) (Hosgood et al., 1995). While the leaf mesophyll structure parameter varies within a range of 1–2 for most of the classes which

Table 4

Land cover-specific inverse estimates of C_m , N and S_z derived from reflectances in the green, red and near-infrared waveband as described in Section 4.4

Land cover class	C_m [g m^{-2}]	N	S_z	C_{ab} [$\mu\text{g cm}^{-2}$]
1	80	1.0	0.9	29 (6.5)
2	30	1.3	0.9	34 (6.1)
3	30	1.75	1.0	36 (5.4)
4	45	1.0	1.0	30 (6.3)
5	25	2.7	0.4	57 (12.3)
6	30	1.3	0.9	32 (4.8)
7	55	1.15	1.0	26 (4.9)
8	45	2.6	0.6	43 (7.3)
9	30	1.9	1.0	36 (3.9)
10	20	2.8	0.6	45 (7.2)
11	30	2.8	1.0	43 (5.0)
12	30	2.2	1.0	39 (4.9)
13	45	1.0	1.0	29 (5.2)

Land cover averaged leaf chlorophyll contents are also provided along with the standard deviation (in the parentheses) of the chlorophyll estimates within each class.

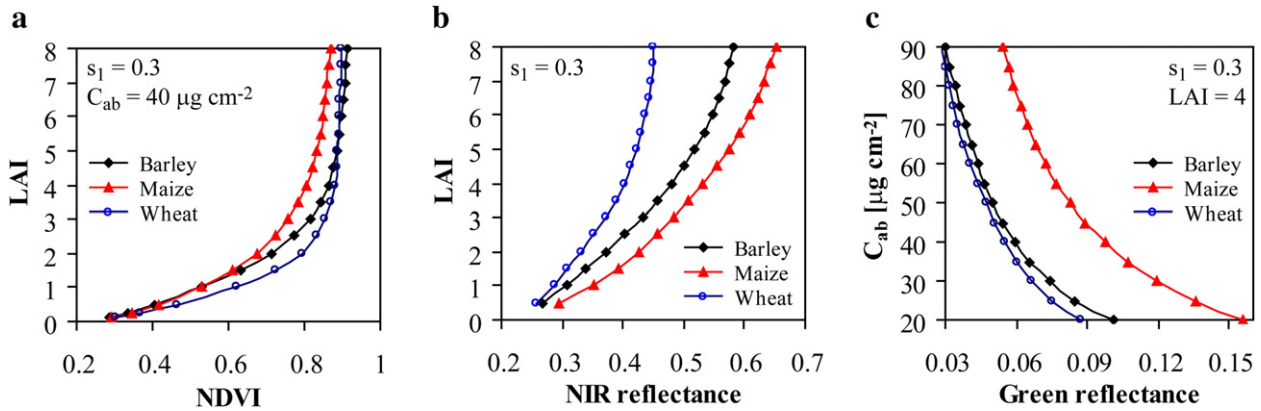


Fig. 5. The effect of contrasting canopy characteristics on LAI–NDVI (a), LAI– ρ_{nir} (b), and $C_{\text{ab}}-\rho_{\text{green}}$ (c) relationships. Sample relationships for wheat, barley and maize are depicted.

suggests a fairly compact mesophyll structure, higher values of N were retrieved for the maize classes. The incorporation of Markov properties of stand geometry in ACRM was found to be important for matching modeled and measured reflectance spectra for the maize classes. In this case, the retrieved values of S_z (0.4 and 0.6 for class 5 and 10, respectively) are consistent with results obtained by Kuusk (1995) and indicate a vertical arrangement of the plant elements. S_z approaches 1.0 for most of the remaining classes indicating homogeneous canopies of randomly positioned leaves.

The effect of contrasting canopy characteristics on LAI– ρ_{nir} , LAI–NDVI and $C_{\text{ab}}-\rho_{\text{green}}$ relationships are demonstrated for wheat, barley and maize in Fig. 5. The Markov properties and leaf structure characteristics of maize cause markedly different responses of LAI to changes in NDVI and ρ_{nir} (Fig. 5a and b) and of C_{ab} to changes in ρ_{green} (Fig. 5c) compared to those of barley and wheat. For example, application of the $C_{\text{ab}}-\rho_{\text{green}}$ relationship for maize causes an increase in leaf chlorophyll of 100% relative to the application of the $C_{\text{ab}}-\rho_{\text{green}}$ relationship for barley (Fig. 5c). While variations in C_m appear to have a fairly minor influence on $C_{\text{ab}}-\rho_{\text{green}}$ relationships, the higher C_m value retrieved for wheat (Table 4) has a large effect on the

derived LAI– ρ_{nir} and LAI–NDVI relationships. The sensitivity to C_m is especially pronounced for the LAI– ρ_{nir} relationship (Fig. 5b) but the decreasing sensitivity of ρ_{nir} to changing leaf biomass as C_m increases also causes a faster saturation of the NDVI signal with increasing LAI (Fig. 5a).

5.2. The effect of site-specific factors

Variations in the class-specific canopy characteristics necessitated the use of a family of land cover dependent LAI– ρ_{nir} , LAI–NDVI and $C_{\text{ab}}-\rho_{\text{green}}$ relationships (Section 5.1) Still, a single relationship for each land cover class may not be sufficient to efficiently describe the spatial variability of the biophysical parameter of interest. Spatial variations in site- (or pixel) specific parameters such as the soil background reflectance signal (s_1), leaf chlorophyll concentration and LAI may require the use of multiple relationships within the same land cover class for an accurate mapping of LAI and C_{ab} .

Fig. 6a illustrates the strong sensitivity of LAI– ρ_{nir} relationships derived for barley to variations in soil reflectance (s_1). Even at high vegetation densities, the soil reflectance signal will impact the LAI predictions as a result of high canopy

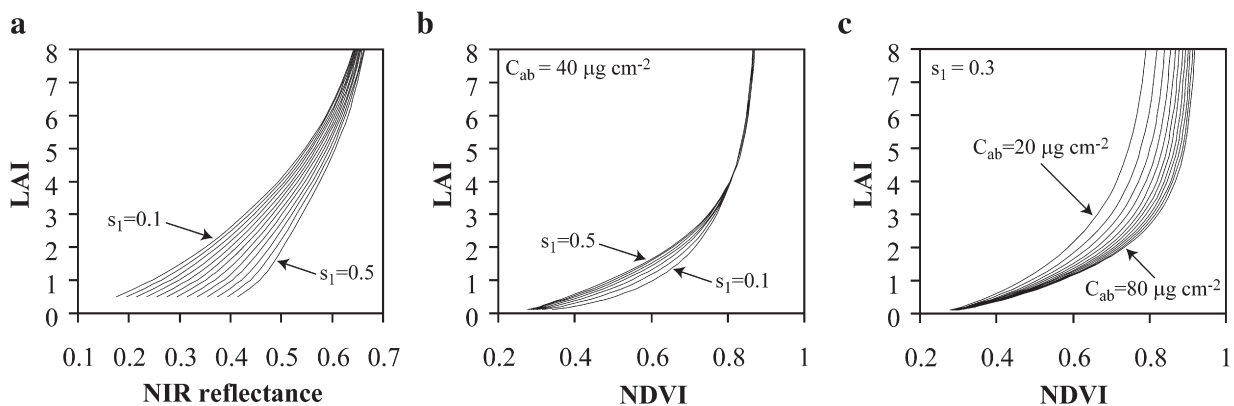


Fig. 6. Effects of site-specific factors, i.e. s_1 and C_{ab} , on LAI– ρ_{nir} (a) and LAI–NDVI (b and c) relationships. The depicted relationships apply to barley fields.

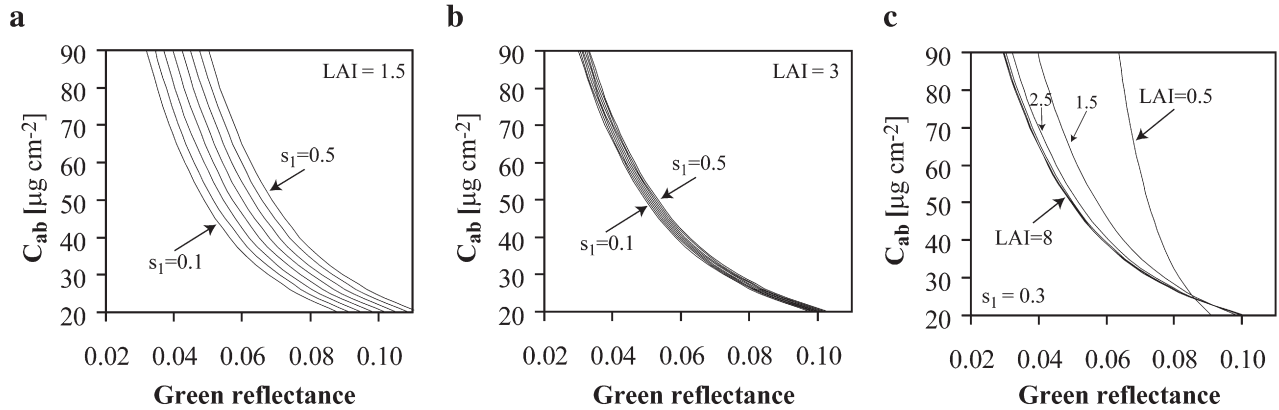


Fig. 7. Effects of variations in the soil background signal (a and b) and LAI (c) on C_{ab} - ρ_{green} relationships. The depicted relationships are representative of barley fields.

penetration capabilities of ρ_{nir} (Fig. 6a). This signifies the importance of employing different LAI- ρ_{nir} relationships for pixels having different soil background reflectance signals. While soil background influences can also be detected in the generated LAI-NDVI relationships, the vegetation index normalization reduces the dependency on s_1 significantly (Fig. 6b). However, the NDVI signal saturates at intermediate vegetation densities and is also highly sensitive to changing chlorophyll concentrations (Fig. 6c). As a result, LAI-NDVI relationships were only applied to pixels with a low vegetation density (LAI < 2) while LAI- ρ_{nir} relationships were adopted for the remaining pixels to exploit the LAI predictive power of ρ_{nir} in densely vegetated areas.

While soil reflectance effects contribute to the green reflectance signal at low vegetation densities (Fig. 7a), the inability of radiometers operating in the green spectrum to sense through a leaf layer (Lillesaeter, 1982) causes a negligible influence of soil reflectance variations already at intermediate vegetation densities (Fig. 7b). Moreover C_{ab} - ρ_{green} relationships are only affected by LAI variations at low to intermediate

vegetation densities (Fig. 7c). Thus, the reliability of the C_{ab} estimates increases with increasing vegetation density as C_{ab} becomes the only factor controlling ρ_{green} at high vegetation density for a given land cover class (Fig. 7c). As a result, a single land cover-specific C_{ab} versus ρ_{green} curve may be used for pixels characterized by a high vegetation density.

5.3. Verification of LAI and leaf chlorophyll estimates

The verification of LAI and C_{ab} estimates against ground measurements was done using the average value of a 2×2 pixel block around the corresponding field plots to account for geolocation error and any mismatch between the point of measurement and the pixel dimensions. The application of the land cover and site-specific LAI-NDVI and LAI- ρ_{nir} relationships resulted in overall good agreements between estimated and measured LAI for barley, wheat and maize sites (Fig. 8) with an overall RMS deviation of 0.74 ($n=19$). Much of the discrepancy is explained by the tendency to underestimate LAI for maize which is characterized by a mean absolute bias of 0.71. The use of LAI- ρ_{nir} relationships for LAI > 2 were found to improve the agreement between in-situ measurements and satellite estimates as the sole use of LAI-NDVI relationships resulted in a RMS deviation of 1.22 (not shown).

Fig. 9a illustrates the spatial distribution of leaf chlorophyll for agricultural land cover classes (Fig. 9b) within a 8×7 km segment of the SPOT image. The map was produced using a family of C_{ab} - ρ_{green} relationships, each being a function of class-specific characteristics (C_m , N , S_z), soil background reflectance signal (s_1) and LAI. The C_{ab} map was prepared as a composite of results from the two SPOT acquisitions (June 22 and September 1) to illustrate spatial variation in C_{ab} of dense vegetation. A large spatial heterogeneity is characteristic of C_{ab} which are seen to vary from 20 to $80 \mu\text{g cm}^{-2}$ (Fig. 9a). For land cover classes such as wheat and barley (which are densely vegetated in June), the average C_{ab} lies in the interval 29 – $39 \mu\text{g cm}^{-2}$ (Table 4). For maize (which are densely vegetated in September), C_{ab} values are considerably higher, i.e. for class 5 and 10, average values of 57 and $45 \mu\text{g cm}^{-2}$ are obtained. A

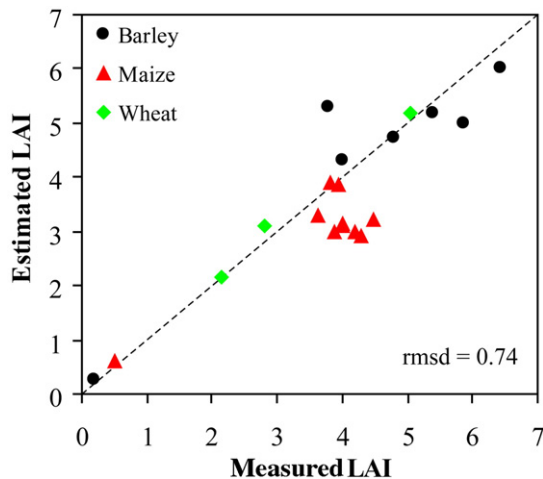


Fig. 8. Verification of estimated LAI against field measured LAI at barley, maize and wheat sites. The dotted line is the 1:1 line.

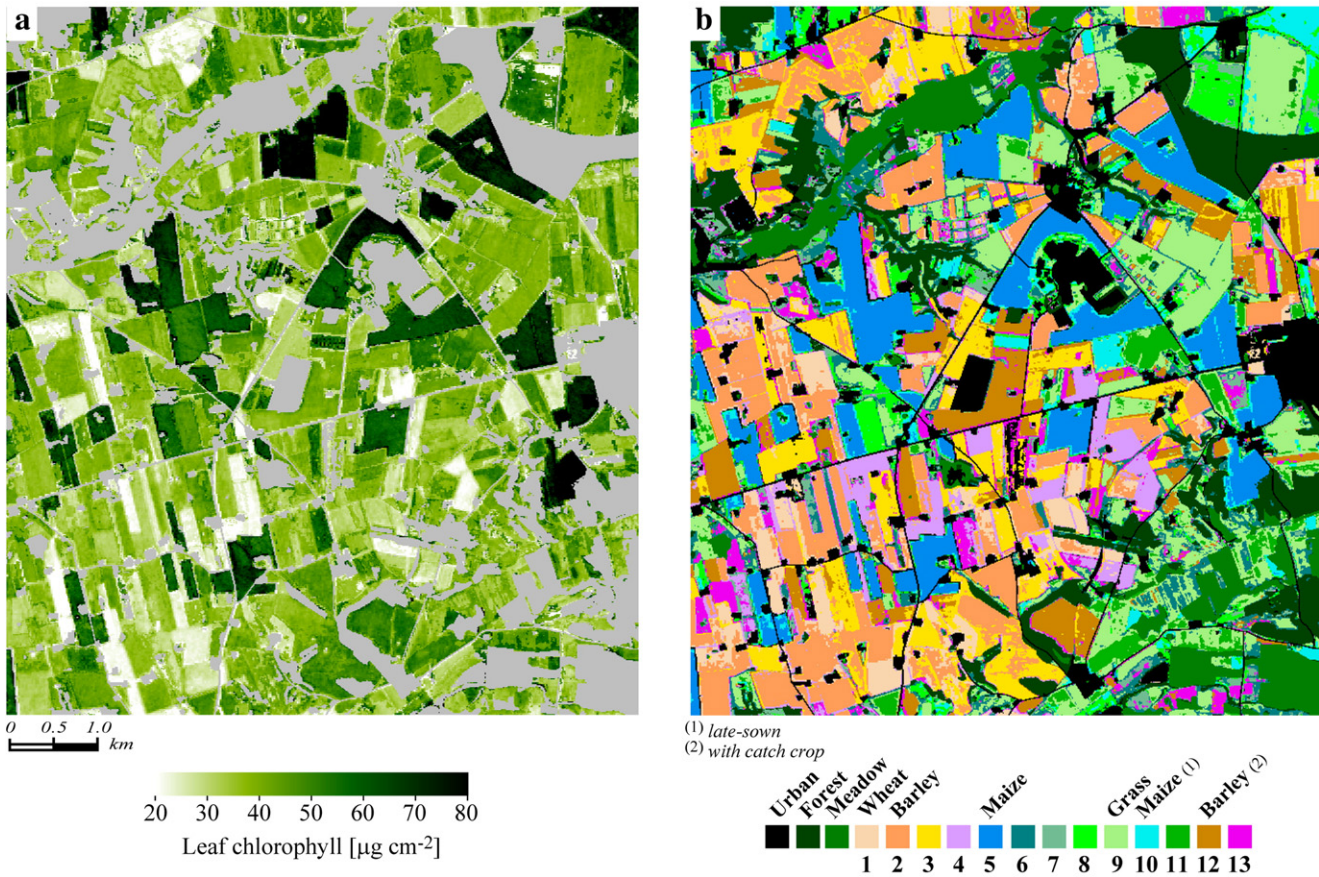


Fig. 9. Spatial distribution of leaf chlorophyll (a) across agricultural land cover classes (b) within a 8×7 km segment of the SPOT image swath. The C_{ab} map (a) represents a composite of results from two SPOT acquisitions (June 22 and September 1) to illustrate leaf chlorophyll contents of dense canopies being in their mid-growing phase (see text).

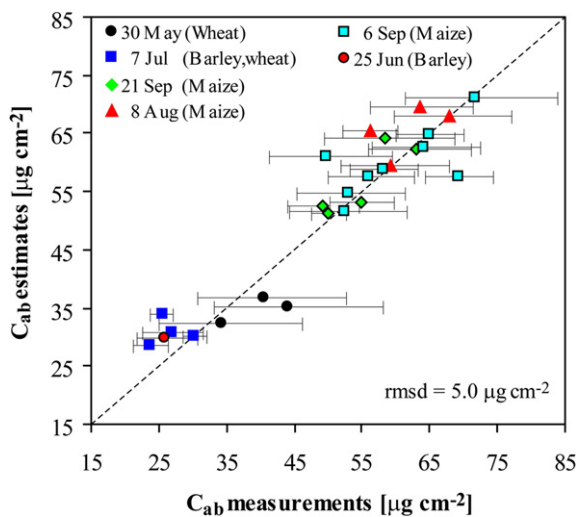


Fig. 10. Verification of remote sensing based leaf chlorophyll (C_{ab}) estimates using field measurements collected at maize, barley and wheat sites within a few days of the two SPOT acquisitions and up to 3 weeks before and after the satellite overpasses (June 22 and September 1). The overall root mean square deviation (rmsd) between estimates and field measurements is listed. The bars represent the standard deviation of the C_{ab} measurements and the dotted line is the 1:1 line.

large within class variability in C_{ab} is evident in both Fig. 9a and Table 4.

The reliability of the C_{ab} estimates was verified for maize, wheat and barley sites. The verification plot (Fig. 10) illustrates a high prediction ability of the C_{ab} - ρ_{green} relationships over a wide range of variation in C_{ab} and a RMS deviation of 5.3 $\mu\text{g cm}^{-2}$ was retrieved when comparing estimates with field measurements collected within a few days of the two SPOT acquisitions (Fig. 10).

While a significant spatial variability was observed for C_{ab} (Fig. 9), measurements of C_{ab} conducted at barley, wheat and maize sites over a wide range of variation in canopy development suggest a fairly constant value of C_{ab} in time for canopies of green leaves in their mid-growing phase (Fig. 11). Thus for any given locality, a single estimate of C_{ab} obtained at some point in the vegetative growth or leaf constant phase could be sufficient and assumed to represent the entire period.

Comparing estimates from the composited C_{ab} map (Fig. 9) with field measurements collected up to 3 weeks before and after the satellite overpass at different wheat, barley and maize sites resulted in a RMS deviation of only 4.9 $\mu\text{g cm}^{-2}$ (Fig. 10). These validation results provide additional confidence in the approach and demonstrate the feasibility of using C_{ab} estimates

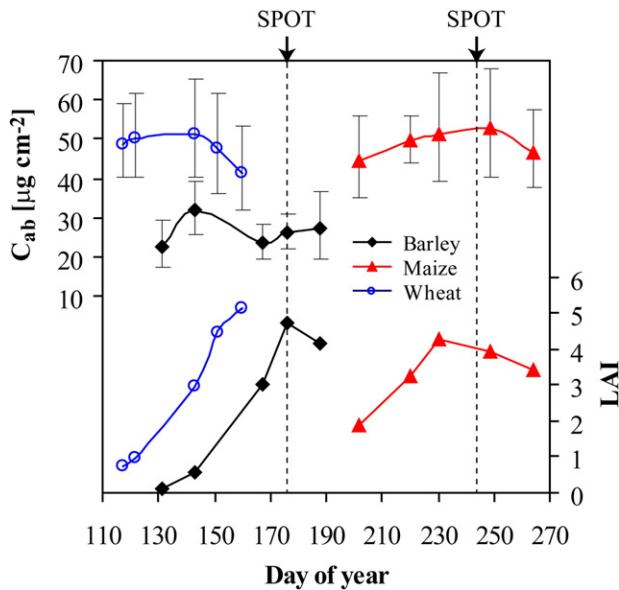


Fig. 11. Temporal progression of measured leaf chlorophyll (C_{ab}) over a wide range of variation in canopy development (LAI). The two SPOT acquisitions are indicated by arrows. The bars represent the standard deviation of the C_{ab} measurements.

derived during peak vegetative conditions as generally representative for the mid-growing vegetative phase.

6. Discussion and conclusions

The use of multiple land cover and site-specific spectral band and index relationships derived largely without the use of in-situ calibration measurements effectuated reliable quantitative estimates of leaf chlorophyll content and LAI for agricultural crops characterized by contrasting architectures and leaf biochemical constituents. The family of $\text{LAI}-\rho_{\text{nir}}$, $\text{LAI}-\text{NDVI}$ and $C_{ab}-\rho_{\text{green}}$ relationships established using inverse and forward CR modeling techniques illustrated the fundamental and well-recognized non-uniqueness of spectral reflectance relationships (e.g. Baret & Guyot, 1991; Broge & Leblanc, 2001; Colombo et al., 2003; Haboudane et al., 2004; Houborg et al., 2007; Zarco-Tejada et al., 2003), and the necessity of using a suite of these simplified relationships for regional-scale mapping applications to take into account soil background effects and variations in canopy characteristics.

Despite of the high vulnerability of ρ_{nir} to variations in background properties even at high vegetation densities, $\text{LAI}-\rho_{\text{nir}}$ relationships were found useful and preferable over $\text{LAI}-\text{NDVI}$ relationships for LAI prediction. The superiority of the $\text{LAI}-\rho_{\text{nir}}$ was due to an effective correction for background influences based on inverse CR modeling techniques and an enhanced sensitivity of ρ_{nir} to LAI for dense vegetative covers. Soil background influences were shown to have a much reduced effect on $C_{ab}-\rho_{\text{green}}$ relationships due to low canopy penetration capabilities of green spectral radiance. Consequently a single land cover-specific C_{ab} versus ρ_{green} curve could be used as a reasonable approximation for pixels characterized by a high vegetation density ($\text{LAI} > 3$). The success of the proposed

background reflectance retrieval scheme relies on (1) the availability of SPOT reflectance observations from fully exposed or sparsely vegetated soil surfaces for each of the land cover classes of interest and (2) the assumption that the soil color of individual pixels is similar at the time of the SPOT acquisitions (Section 4.3). The latter point is only true when the humus content remains unchanged and the topsoil is equally dry in all scenes. As the transition phase from moist to dry topsoil is of relatively short duration (e.g. Sellers et al., 1997), most clear-sky satellite acquisitions are believed to be applicable unless immediately succeeding a precipitation event.

SPOT reflectance observations of peak vegetative covers were required for the inverse retrieval of spatially and temporally invariant canopy parameters for each land cover class (Section 4.4). While the retrieval scheme solves automatically for the dry matter content (C_m), leaf mesophyll structure (N) and Markov clumping characteristics (S_z), leaf inclination angles (θ_1) are either parameterized from a priori information or fixed assuming a spherical leaf angle distribution (LAD). Remote sensing based CR modeling studies typically assume a spherical leaf orientation (Fang & Liang, 2005; Fang et al., 2003; Haboudane et al., 2004) as a spherical LAD is a reasonable approximation for a wide range of crops (Campbell & Norman, 1998). However θ_1 is an influential factor in visible and near-infrared reflectance spectra (Bacour et al., 2002) and increasing θ_1 from a planophile to an erectophile canopy causes an increase in the sensitivity of reflectance spectra to θ_1 especially when viewed from an oblique angle (Houborg et al., 2007). The use of directional data, acquired from multi-angle sensors like the Multi-angle Imaging SpectroRadiometer (MISR) or from multi-temporal acquisitions from sensors with a wide range in viewing angles, in addition to extra wavebands located in the mid-infrared spectrum could probably aid the inferences of canopy structure parameters such as θ_1 (Eklundh et al., 2001; Houborg et al., 2007). This would reduce modeling errors caused by departures from a spherical LAD.

The inverse estimation of C_m , N and S_z was made feasible by assuming invariance of these parameters within well-defined spectrally separate land cover classes, and by allowing the information content provided by a land cover-specific spatial reflectance dataset to be exploited. The estimates of S_z were in accordance with observations demonstrating the distinct Markov properties of maize canopies (Kuusk, 1995; Ross, 1981) and the more random position of leaves in canopies of wheat and barley (Campbell & Norman, 1998). The inverse retrieval of C_m and N is complicated by the very similar response of ρ_{green} , ρ_{red} and ρ_{nir} to variations in C_m and N , which makes it difficult to separate the contributions of C_m and N to the reflectance signal (Jacquemoud et al., 2000). For the maize classes, the retrieved N values (2.7–2.8) disagree with the compact mesophyll structure of monocotyledon leaves (e.g. maize) (Jacquemoud & Baret, 1990) and the C_m values lie at the low extreme of range values observed for maize in the LOPEX'93 dataset (Hosgood et al., 1995). The reflectance response to the combination of a high N and low C_m value is a significant increase of ρ_{nir} and a slight increase of ρ_{green} and ρ_{red} (Houborg et al., 2007). Possibly, the 'unrealistic' N and C_m

values for maize are the result of the CR model trying to match reflectance spectra influenced by factors currently not properly described by the CR model. Maize flowering or the existence of yellow leaves in the canopy could be possible explanations as both factors will cause an increase of reflectance in the visible and near-infrared wavelengths. This may explain the LAI underestimation for maize (Fig. 8) as an increase of LAI causes a decrease of visible waveband reflectances (Houborg et al., 2007) thereby increasing the deviation between observed and modeled reflectances.

While leaf chlorophyll concentrations are known to decrease markedly for semi-green and yellow leaves (Boegh et al., 2002), our data suggested a fairly conservative temporal evolution of C_{ab} for canopies of green leaves during the mid-growing vegetation phases. Accordingly single pixel-wise estimates of C_{ab} derived during conditions of high density green vegetation, when the sensitivity of ρ_{green} to changing leaf chlorophyll concentrations is maximized, might be assumed representative of the vegetative growth and leaf constant phases for the studied crop types. This assumption is viable because of non-stressed environmental conditions whereas water stress and nitrogen deficiency may cause a decrease of leaf chlorophyll concentrations (Carter, 1994). The temporal variability in C_{ab} and LAI may be modeled by applying the family of generated spectral relationships to SPOT reflectance observations acquired at intermediate vegetation stages between the 'bare soil' and dense vegetation acquisition. This is feasible as the land cover-specific vegetation and site-specific soil parameters are assumed temporally invariant.

The correlation of leaf chlorophyll with leaf nitrogen is well known (e.g. Blackburn, 1998; Boegh et al., 2002; Yoder & Pettigrew-Crosby, 1995) and estimates of leaf nitrogen have been converted to estimates of the maximum catalytic capacity of Rubisco (V_m) (Boegh et al., 2002; De Pury & Farquhar, 1997; Haxeltine & Prentice, 1996; Nijs et al., 1995), which is a key variable in the widely used leaf photosynthesis model of Farquhar et al. (1980). V_m describes the biochemical capacity of leaves to assimilate CO_2 and a successful implementation of the Farquhar leaf photosynthesis model in Soil Vegetation Atmospheric Transfer (SVAT) schemes requires V_m to be accurately assessed (Houborg & Soegaard, 2004). The significant spatial variability in leaf chlorophyll observed for the study region stresses the need for a spatial parameterization of the correlated variable, V_m , for the establishment of regional carbon budgets, and accurate predictions of leaf chlorophyll from remotely sensed data could be a step towards obtaining this important goal.

In principle, the presented biophysical parameter scheme can be directly implemented and run for any agricultural region on the earth due to the independency on in-situ measurements. The methodology requires at least two clear-sky SPOT scenes to represent conditions of dense green vegetation and bare soil respectively for each of the agricultural crops of interest. The robustness of the scheme also relies on readily available and accurate atmospheric profile data for the conversion of SPOT radiances into surface reflectances, and the study demonstrated a promising potential of data from Aqua AIRS.

To summarize, the scheme was made completely automated and image-based by using aerosol concentrations and atmospheric profile data from Aqua MODIS and AIRS which are available globally every 1–2 day for atmospheric correction purposes, (2) an unsupervised isodata classification approach for the separation of spectrally homogeneous land cover classes, (3) a soil map, and (4) by solving for the soil background reflectance signal, leaf mesophyll structure, dry matter content, Markov clumping parameter, leaf chlorophyll content and leaf area index using innovative inverse and forward CR modeling techniques without the use of a priori ground based information.

While the flexibility of the approach and independency of in-situ data allow for easy model implementation anywhere, more validation studies are needed to evaluate the usefulness and limitations of the approach for other environments and species compositions.

Acknowledgements

The present study was conducted within the project "Remote sensing of leaf nutrition for biochemical and environmental modeling of crop photosynthesis" which was funded by the Danish Agricultural Research Council. The authors wish to thank Dr. Andres Kuusk for providing the latest ACRM source code. Free access to SPOT data was provided by the OASIS programme (*Optimizing Access to SPOT Infrastructure for Science*) which is coordinated by CNES and financed by the European Commission (<http://medias.obs-mip.fr/oasis/>).

References

- Atzberger, C. (2004). Object-based retrieval of biophysical canopy variables using artificial neural nets and radiative transfer models. *Remote Sensing of Environment*, 93, 53–67.
- Bacour, C., Baret, F., Beal, D., Weiss, M., & Pavageau, K. (2006). Neural network estimation of LAI, fAPAR, fCover and LAI \times C_{ab} from top of canopy MERIS reflectance data: Principles and validation. *Remote Sensing of Environment*, 105, 313–325.
- Bacour, C., Jacquemoud, S., Leroy, M., Hauteceur, O., Weiss, M., Prévot, L., et al. (2002). Reliability of the estimation of vegetation characteristics by inversion of three canopy reflectance models on airborne POLDER data. *Agronomie*, 22, 555–565.
- Baret, F. (1991). Vegetation canopy reflectance: Factors of variation and application for agriculture. In D. Hunt (Ed.), *Physical measurements and signatures in remote sensing* (pp. 145–167). France: Courchevel.
- Baret, F., & Fourty, T. (1997). Radiometric estimates of nitrogen status in leaves and canopies. In G. Lemaire (Ed.), *Diagnosis of the nitrogen status in crops* (pp. 201–227). Berlin: Springer.
- Baret, F., & Guyot, G. (1991). Potentials and limits of vegetation indices for LAI and APAR assessment. *Remote Sensing of Environment*, 35, 161–173.
- Blackburn, G. A. (1998). Quantifying chlorophyll and carotenoids at leaf and canopy scales: an evaluation of some hyperspectral approaches. *Remote Sensing of Environment*, 66, 273–285.
- Boegh, E., Soegaard, H., Broge, N., Hasager, C. B., Jensen, N. O., Schelde, K., et al. (2002). Airborne multispectral data for quantifying leaf area index, nitrogen concentration, and photosynthetic efficiency in agriculture. *Remote Sensing of Environment*, 81, 179–193.
- Boegh, N. M., & Leblanc, E. (2001). Comparing predictive power and stability of broadband and hyperspectral vegetation indices for estimation of green leaf area index and canopy chlorophyll density. *Remote Sensing of Environment*, 76, 156–172.

- Campbell, G. S. (1990). Derivation of an angle density function for canopies with ellipsoidal leaf angle distributions. *Agricultural and Forest Meteorology*, 49, 173–176.
- Campbell, G. S., & Norman, J. M. (1998). *An introduction to environmental biophysics*. New York: Springer-Verlag 286 pp.
- Carter, G. A. (1994). Ratios of leaf reflectances in narrow wavebands as indicators of plant stress. *International Journal of Remote Sensing*, 15, 697–704.
- Colombo, R., Bellingeri, D., Fasolini, D., & Marino, C. M. (2003). Retrieval of leaf area index in different vegetation types using high resolution satellite data. *Remote Sensing of Environment*, 86, 120–131.
- Combal, B., Baret, F., Weiss, M., Trubuil, A., Macé, D., Pragnère, A., et al. (2002). Retrieval of canopy biophysical variables from bidirectional reflectance using prior information to solve the ill-posed inverse problem. *Remote Sensing of Environment*, 84, 1–15.
- Danish Areal Information System (2000). AIS. www.dmu.dk
- Danish Institute of Agricultural Sciences (1996). Soil map. www.agrsci.dk
- Denmark's Meteorological Institute (2006). www.dmi.dk
- De Pury, D. G. G., & Farquhar, G. D. (1997). Simple scaling of photosynthesis from leaves to canopies without the errors of big-leaf models. *Plant, Cell and Environment*, 20, 537–557.
- Eklundh, L., Harrie, L., & Kuusk, A. (2001). Investigating relationships between Landsat ETM+ sensor data and leaf area index in a boreal conifer forest. *Remote Sensing of Environment*, 78, 239–251.
- Fang, H., & Liang, S. (2005). A hybrid inversion method for mapping leaf area index from MODIS data: Experiments and application to broadleaf and needleleaf canopies. *Remote Sensing of Environment*, 94, 405–424.
- Fang, H., Liang, S., & Kuusk, A. (2003). Retrieving leaf area index using a genetic algorithm with a canopy radiative transfer model. *Remote Sensing of Environment*, 85, 257–270.
- Farquhar, G. D., von Caemmerer, S., & Berry, J. A. (1980). A biochemical model of photosynthetic CO₂ assimilation in leaves of C₃ species. *Planta*, 149, 603–619.
- Fetzer, E. J., Eldering, A., Fishbein, E. F., Hearty, T., Irion, W. F., & Kahn, B. (2005). *Validation of AIRS/AMSU/HSB core products for Data Release Version 4.0*. Available online at http://disc.gsfc.nasa.gov/AIRS/documentation/v4_docs/V4.0_Validation_Report.pdf
- Gitelson, A. A., Kaufman, Y. J., & Merzlyak, M. N. (1996). Use of a green channel in remote sensing of global vegetation from EOS-MODIS. *Remote Sensing of Environment*, 58, 289–298.
- Gitelson, A. A., Viña, A., Ciganda, V., & Rundquist, D. C. (2005). Remote estimation of canopy chlorophyll content in crops. *Geophysical Research Letters*, 32, L08403. doi:10.1029/2005GL022688
- Gobron, N., Pinty, B., & Verstraete, M. M. (1997). Theoretical limits to the estimation of the leaf area index on the basis of visible and near-infrared remote sensing data. *IEEE Transactions on Geoscience and Remote Sensing*, 35(6), 1438–1445.
- Haboudane, D., Miller, J. R., Pattey, E., Zarco-Tejada, P. J., & Strachan, I. B. (2004). Hyperspectral vegetation indices and novel algorithms for predicting green LAI of crop canopies: Modeling and validation in the context of precision agriculture. *Remote Sensing of Environment*, 90, 337–352.
- Haxeltine, A., & Prentice, I. C. (1996). A general model for the light-use efficiency of primary production. *Functional Ecology*, 10, 551–561.
- Hosgood, B., Jacquemoud, S., Andreoli, G., Verdebout, J., Pedrini, G., & Schmuck, G. (1995). Leaf Optical Properties Experiment 93 (LOPEX93). *European Commission, Joint Research Centre, Institute for Remote Sensing Applications, Report EUR 16095 EN*.
- Houborg, R. M., & Soegaard, H. (2004). Regional simulation of ecosystem CO₂ and water vapor exchange for agricultural land using NOAA AVHRR and Terra MODIS satellite data. Application to Zealand, Denmark. *Remote Sensing of Environment*, 93, 150–167.
- Houborg, R., Soegaard, H., & Boegh, E. (2007). Combining vegetation index and model inversion methods for the extraction of key vegetation biophysical parameters using Terra and Aqua MODIS reflectance data. *Remote Sensing of Environment*, 106, 39–58.
- Houborg, R., Soegaard, H., Emmerich, W., Moran, S. (in press). Inferences of all-sky solar irradiance using Terra and Aqua MODIS satellite data. *International Journal of Remote Sensing*.
- Huete, A., Didan, K., Miura, T., Rodriguez, E. P., Gao, X., & Ferreira, L. G. (2002). Overview of the radiometric and biophysical performance of the MODIS vegetation indices. *Remote Sensing of Environment*, 83, 195–213.
- Iqbal, H. (1983). *An introduction to solar radiation*. New York: Academic Press 390 pp.
- Jacquemoud, S., & Baret, F. (1990). PROSPECT: A model of leaf optical properties spectra. *Remote Sensing of Environment*, 34, 75–91.
- Jacquemoud, S., Baret, F., Andrieu, B., Danson, F. M., & Jaggard, K. (1995). Extraction of vegetation biophysical parameters by inversion of the PROSPECT+ SAIL models on sugar beet canopy reflectance data. Application to TM and AVIRIS sensors. *Remote Sensing of Environment*, 52, 163–172.
- Jacquemoud, S., Bacour, C., Poilvé, H., & Frangi, J. -P. (2000). Comparison of four radiative transfer models to simulate plant canopies reflectance: Direct and inverse mode. *Remote Sensing of Environment*, 74, 471–481.
- Kaufman, Y. J., & Tanré, D. (1998). Algorithm for remote sensing of tropospheric aerosol from MODIS (ATBD). http://modis.gsfc.nasa.gov/data/atbd/atbd_mod02.pdf
- Kaufman, Y. J., Tanré, D., Remer, L. A., Vermote, E. F., Chu, A., & Holben, B. N. (1997). Operational remote sensing of tropospheric aerosol over land from EOS moderate resolution imaging spectroradiometer. *Journal of Geophysical Research*, 102, 17051–17067.
- Knyazikhin, Y., Martonchik, J. V., Diner, D. J., Myneni, R. B., Verstraete, M., Pinty, B., et al. (1998). Estimation of vegetation canopy leaf area index and fraction of absorbed photosynthetically active radiation from atmosphere-corrected MISR data. *Journal of Geophysical Research*, 103(D24), 32239–32256.
- Knyazikhin, Y., Martonchik, J. V., Myneni, R. B., Diner, D. J., & Running, S. W. (1998). Synergistic algorithm for estimating vegetation canopy leaf area index and fraction of absorbed photosynthetically active radiation from MODIS and MISR data. *Journal of Geophysical Research*, 103(D24), 32257–32276.
- Kuusk, A. (1995). A Markov chain model of canopy reflectance. *Agriculture and Forest Meteorology*, 76, 221–236.
- Kuusk, A. (2001). A two-layer canopy reflectance model. *Journal of Quantitative Spectroscopy & Radiative Transfer*, 71, 1–9.
- Kuusk, A. (2003). *Two-layer canopy reflectance model*. ACRM user guide 21 pp.
- Lillesaeter, O. (1982). Spectral reflectance of partly transmitting leaves: Laboratory measurements and mathematical modeling. *Remote Sensing of Environment*, 12, 247–254.
- Markwell, J., Ostermann, J. C., & Mitchell, J. L. (1995). Calibration of the Minolta SPAD-502 leaf chlorophyll meter. *Photosynthesis Research*, 46, 467–472.
- Moran, R. (1992). Formulae for determination of chlorophyllous pigments extracted with *N,N*-dimethylformamide. *Plant Physiology*, 69, 1376–1381.
- Nijs, I., Behaeghe, T., & Impens, I. (1995). Leaf nitrogen content as a predictor of photosynthetic capacity in ambient and global change conditions. *Journal of Biogeography*, 22, 177–183.
- Porra, R. J., Thompson, W. A., & Kriedemann, P. E. (1989). Determination of accurate extinction coefficients and simultaneous equations for assaying chlorophylls *a* and *b* extracted with four different solvents: Verification of the concentration of chlorophyll standards by atomic absorption spectroscopy. *Biochimica et Biophysica Acta*, 975, 384–394.
- Price, J. C. (1990). On the information content of soil reflectance spectra. *Remote Sensing of Environment*, 33, 113–121.
- Ross, J. (1981). *The radiation regime and architecture of plant stands*. The Hague: Dr W. Junk Publishers 388 pp.
- Sellers, P. J., Heiser, M. D., Hall, F. G., Verma, S. B., Desjardins, R. L., Schuep, P. M., et al. (1997). The impact of using area-averaged land surface properties – Topography, vegetation condition, soil wetness – In calculations of intermediate scale (approximately 10 km(2)) surface–atmosphere heat and moisture fluxes. *Journal of Hydrology*, 190(3–4), 260–301.
- Tou, J. T., & Gonzalez, R. C. (1974). *Pattern recognition principles*. Reading, Massachusetts: Addison-Wesley Publishing Company 377 pp.
- Tucker, C. J. (1980). Remote sensing of leaf water content in the near infrared. *Remote Sensing of Environment*, 10, 23–32.
- Verhoef, W., & Bach, H. (2003). Simulation of hyperspectral and directional radiance images using coupled biophysical and atmospheric radiative transfer models. *Remote Sensing of Environment*, 87, 23–42.

- Vermote, E. F., El Saleous, N. Z., & Justice, C. O. (2002). Atmospheric correction of MODIS data in the visible to middle infrared: First results. *Remote Sensing of Environment*, 83, 97–111.
- Vermote, E. F., & Vermeulen, A. (1999). Atmospheric correction algorithm: Spectral reflectances (MOD09). Algorithm Technical Background Document (ATBD). http://modis.gsfc.nasa.gov/data/atbd/atbd_mod08.pdf
- Walthall, C., Dulaney, W., Anderson, M., Norman, J., Fang, H., & Liang, S. (2004). A comparison of empirical and neural network approaches for estimating corn and soybean leaf area index from Landsat ETM+ imagery. *Remote Sensing of Environment*, 92, 465–474.
- Weiss, M., & Baret, F. (1999). Evaluation of canopy biophysical variable retrieval performances from the accumulation of large swath satellite data. *Remote Sensing of Environment*, 70, 293–306.
- Weiss, M., Baret, F., Myneni, R. B., Pragnère, A., & Knyazikhin, Y. (2000). Investigation of a model inversion technique to estimate canopy biophysical variables from spectral and directional reflectance data. *Agronomie*, 20, 3–22.
- Yoder, B. J., & Pettigrew-Crosby, R. E. (1995). Predicting nitrogen and chlorophyll concentrations from reflectance spectra (400–2500 nm) at leaf and canopy scales. *Remote Sensing of Environment*, 49, 81–91.
- Zarco-Tejada, P. J., Rueda, C. A., & Ustin, S. L. (2003). Water content estimation in vegetation with MODIS reflectance data and model inversion methods. *Remote Sensing of Environment*, 85, 109–124.